Modelling Acoustic Emissions Generated by Tribological Behaviour of Mechanical Seals for Condition Monitoring and Fault Detection

Hossein Towsyfyan[1*], Fengshou Gu[2], Andrew D Ball[2], Bo Liang[2]

1. Institute of Sound and Vibration Research (ISVR), University of Southampton, UK
2. School of Computing and Engineering, University of Huddersfield, UK

Abstract

Acoustic emission (AE) signals are useful for the condition monitoring of mechanical seals as tribological regimes affect the AE signatures. In this paper the investigation develops a mathematical model that can predict the energy of an AE signal under different tribological regimes. The developed model has been validated with experimental studies and satisfactory results have been perceived. Therefore, the model has strong potential to be used to obtain tribological behavior of mechanical seals and hence develop a reliable and accurate condition monitoring system under varying operating conditions.

Key words: Tribological regimes, Mechanical seals, Acoustic emission

1 Introduction

Acoustic emission (AE), as an attractive method, has been proven to be sensitive to tribological behaviour of rotating machines such as journal bearings and mechanical seals. This includes identification of lubrication regimes [1,2], monitoring the sliding contact [3,4], investigation of the effect of working parameters [5, 6] and fault detection [7,8]. Since AE sensors measure the actual source mechanism itself, the application of acoustic emission for condition monitoring of other tribosystems such as wind turbines [9,10], gearboxes [11,12] and rolling element bearings [13,14] is also very popular.

As a tribosystem, Fig.1, mechanical seals are exposed to widely varying operating conditions, and hence may experience different tribological regimes i.e. boundary lubrication (BL), mixed lubrication (ML) and hydrodynamic lubrication (HL) regime depending on the operating conditions. The effect of operating conditions (e.g. load, rotational speed and viscosity) on tribological behavior of mechanical seals is characterised by well-known Stribeck curve, where

* Corresponding Author E-mail: H.Towsyfyan@soton.ac.uk

coefficient of friction, f, is plotted as a function of dimensionless duty parameter, G, as shown schematically in Fig. 2.

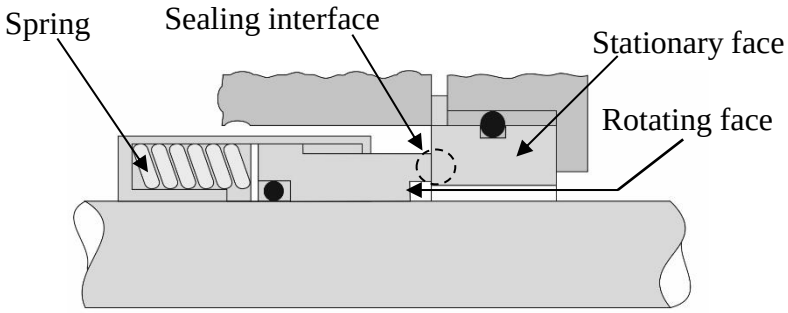

Fig.1. Schematic illustration of mechanical seals

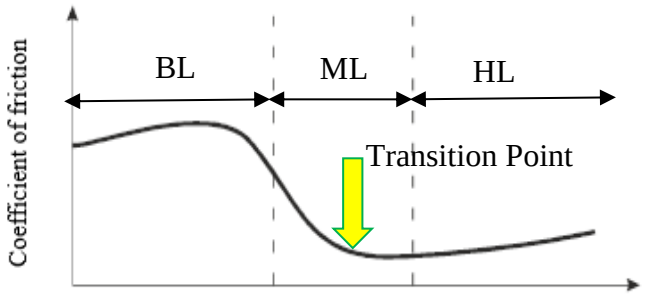

$$G = \frac{\text{Viscosity} \times \text{Speed}}{\text{Load}}$$

Fig.2. Stribeck curve

Three main mechanisms may contribute to generation of tribological AEs in mechanical seals. In the hydrodynamic lubrication regime, the main sources of AE are viscous friction due to the shearing of lubricant layers at the sealing interface as well as elastic deformation of asperities due to flow induced vibrations. The latter type of AE source can be understood to be the effect of fluid stress field that cause an alternation between asperity deformation and recovery as moving asperities approach and leave the stationary asperities. Fluid stress field changes due to the fact that fluid pressure increases when the asperity is approached and decreases when the asperity is left behind [17, 18]. This leads to the development of a vibratory behaviour in the surface asperities that exhibits an analogous behaviour with direct asperity contact where local pressure fields develop around the surface asperities [19]. Under this condition ideally no asperity contact occurs, but the dynamic bending and reclamation of asperities produce AE waves due to the interactions between the micro asperities and high-pressure fluid flows, as illustrated in Fig.3 (a). Studies conducted by H. Towsyfyan [20] proved that flow induced vibration of asperities results in the generation of AE waves along with frictional heat. Details of this mechanism is beyond the concept of this paper, interested readers may refer to references [20-23] for a

comprehensive review and detailed discussion. At the meantime friction-induced emissions in the lubricant film, confined between the mating surfaces, may occur which is referred to as viscous friction in this work. The friction response of such confined layers under shear stress can be complex and depends on the operating conditions, the nature of the surfaces and their mechanical and topographic characteristics, as well as the nature and shape of the confined fluid molecules [24-27]. These responses transmit energy from the flow to the surrounding solids as well as dissipating the kinetic energy of the flow as viscous shear stresses perform work. By either increasing the pressure or decreasing the speed, as it is characterised by Stribeck curve, the lubrication status becomes mixed lubrication or boundary lubrication regime in which the collisions of asperities can be more pronounced and thus produce AE responses that is well documented in the literature [28, 29]. As shown schematically in Fig.3 (b), the sliding movement of mating faces causes a dynamic bending load on contact asperities when a pair of asperities approach each other which then release when they leave the interaction zone.

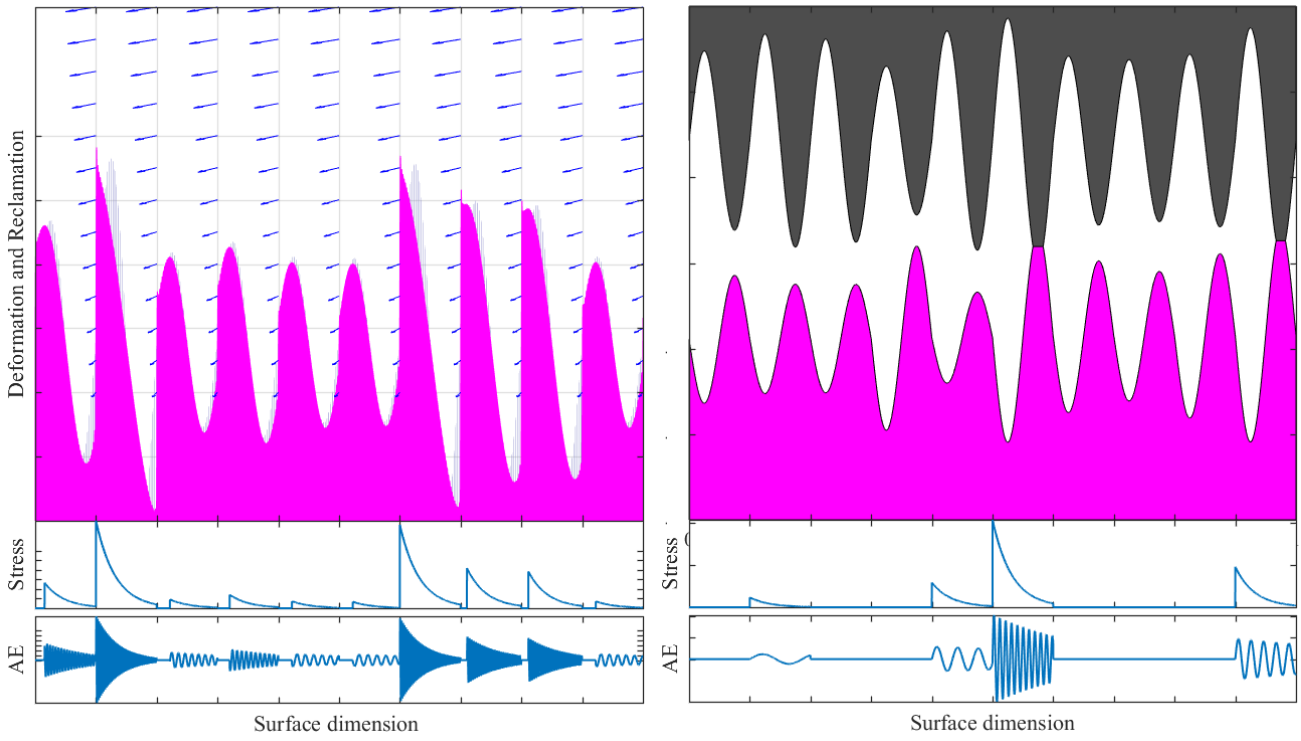

(a) (b)

Fig. 3. Elastic deformation of asperities in the sealing gap (a) Flow induced deformations. (b) Direct asperity contact

Above understandings reveal there is a good correlation between the working parameters of mechanical seals and AE signatures. However, the development of a theoretical model that can predict the level of an AE signal under different lubrication condition of mechanical seals, as a primary phase for accurate seal monitoring, has not yet been reported. This is of high importance to avoid premature failures of mechanical seals due to the transition between different tribological regimes. Moreover, any deviation from the predicted trend can be considered as a developing fault that is essential in many engineering applications. Therefore, it is necessary to model the tribological behaviour of mechanical seals operating based on nonlinear coupling between the sealed fluid and surface dynamics in order to develop more advanced AE based diagnostic technologies to improve the reliability of rotating machines operating with mechanical seals. This is more critical in the mixed and hydrodynamic lubrication regimes where friction values depend on many complicated parameters such as roughness height, seal face material, contact load and sliding speed [15, 16].

This paper attempts to fill this gap and presents a model to correlate the level of AE signals to the tribological behaviour of mechanical seals based on the strain energy released during elastic deformation of surface asperities as well as viscous friction in the lubricant fluid. With the help of this model, it is possible to evaluate the lubrication condition through the AE measurement.

3. Mathematical Modelling

Several studies demonstrate that attempts have been made for modelling of AE excitations generated by direct asperity contact, which is considered conventionally as the main cause of all failures in sliding contact of mating surfaces [28-31]. AE signals generated during sliding contact of rotating machines are modelled mathematically using two general approaches. The first approach is integrating the friction force over the sliding distance $\int F\ ds$. [32- 34]. The sliding distance in the collision of a pair of asperities is calculated based on the radius of the circular contact region (green area in Fig. 4). Since it is not possible to measure the actual radius of the circular contact region nor accurately calculate it based on the available theories, presenting the sliding distance in this way has not been well developed. Moreover, for micro scale contacts, the importance of the effect of adhesion on the contact area [31] is not considered in this approach and for that reason has been used less frequently.

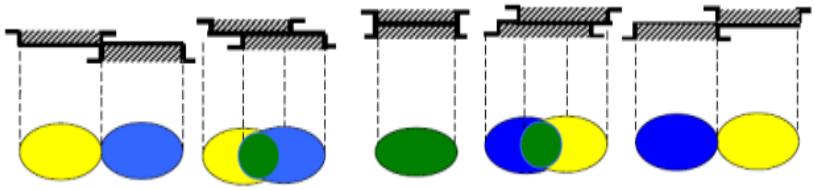

Fig. 4. The concept of sliding distance in asperity contact

Another approach is based on strain energy released during elastic deformation of the asperities. F. Y. Edward et al. [17] used the integration of contact load over elastic deflection of the asperities, $\int W\, d\delta$, to model the stored strain energy during sliding contact of mating surfaces as shown schematically in Fig. 5. In 2017, Sharma and Parey [29] applied this method to model the stored elastic energy for the asperity contact between the surfaces of inner race and outer race rolling element. In present paper, the latter approach is followed. However, the model will be developed based on the dynamic bending of surface asperities that is more consistent with the physics of sliding contact in mechanical seals.

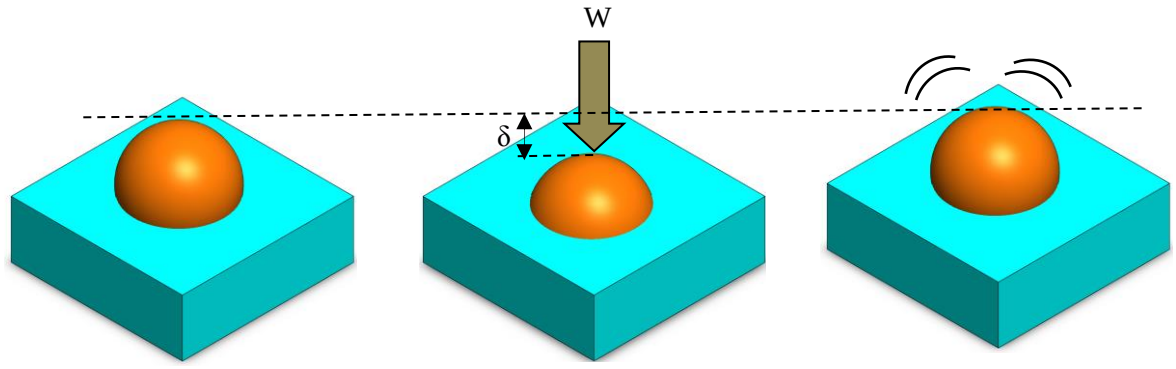

(a) Asperity in rest (b) Compressed asperity (c) Energy released

Fig. 5. The concept of strain energy released in sliding contact

Beside modelling the tribological AEs, it is also important to characterise them based on suitable features extracted from AE waveform. Research has been reported in the literature showing that a strong relationship exists between the root mean square (RMS) value of the AE signals, V_{rms}, and the multiple interactions between AE sources in the sliding contact [35-39]. This correlation has been demonstrated theoretically in the work of Sharma and Parey [29] as well as F.Y. Edward et al. [30] where it has been proven that the equation bellow is mathematically valid:

$$V_{rms} = \sqrt{\dot{U}_{AE}} \tag{1}$$

where $\dot{U}_{AE}$ is the energy excited by AE mechanisms.

3.1 Deformation Mechanic of Randomly Rough Surfaces

Based on the Greenwood and Williamson [40] approach the contact of two engineering flat surfaces with roughness Rq_1 and Rq_2 can be estimated by converting it into the contact between two surfaces; one is assumed smooth and the other is a rough surface with equivalent roughness $R_q = \sqrt{{R_{q1}}^2 + {R_{q2}}^2}$. Moreover, the probability that an asperity has a height between z and $z + dz$ above the reference plane is defined as $f(z)$. Therefore, if two surfaces come together until their reference planes are separated by a distance d then there will be a contact (shaded in Fig. 6) and the load is supported by those equivalent asperities whose height are originally greater than d. Thus the probability of making contact at any given asperity of height z is [41, 42]:

$$p(z > d) = \int_d^\infty f(z)\,dz \tag{2}$$

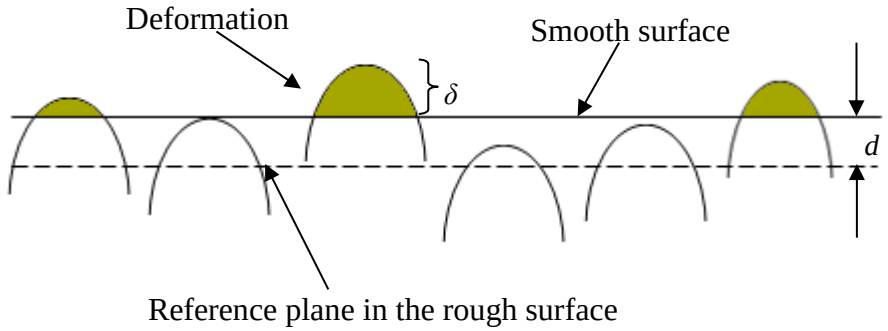

Fig. 6. The Greenwood and Williamson model for contact

The maximum deflection in the contact area , δ, as well as other deformation parameters and their relations are given by Hertz Equations [28-30,40,42,43]. It was assumed that the number of asperities per unit area is D, thus the expected number of contacts in any unit area is given by:

$$n = D\int_d^\infty f(z)\,dz \tag{3}$$

In case of flow induced asperity deformations, the contact mechanics of rough surfaces is not applicable. Hence, in this paper, the Greenwood and Williamson theory of contact model is adopted with new definitions. Based on Fig. 6, if the sealing gap is filled with the pressurised sealed fluid that moves with speed of V and the reference plane of the mating faces are separated by a distance d then there will be some flow induced deformations in those asperities whose height are originally greater than d. Hence the Eqs. (2) and (3) can be applied with the new

definition. Here $p(z > d)$ is the probability of asperity deformation due to fluid flow at any given height of asperity and n is the expected number of elastic asperity deformations in any unit area.

3.2 Modelling Asperity Elastic Deformation

In this section the AE energy discharge due to elastic deformation of equivalent asperities adopted from previous section is modelled step by step. This includes both asperity-asperity and fluid-asperity interactions.

3.2.1 Calculation the friction force acting on a single asperity

Conventionally the tangential friction force in the sliding direction between a pair of asperities is described as follows [15]:

$$F = \iint \tau \, dA \tag{4}$$

where τ is shear stress that acts on the area of A from a single asperity. For the remainder of the paper, A is substituted with πr^2 where r is the average radius of an equivalent asperity given by Hertz theory. The shear stress in asperity-asperity (*a*-*a*) and fluid-asperity (*f*-*a*) interactions can be expressed by Eqs. (5) and (6) respectively:

$$\tau_{a-a} = f \sigma \tag{5}$$

$$\tau_{f-a} = \mu \frac{V}{h} \tag{6}$$

where f, σ, μ and h are the coefficient of friction, the normal stress in a single asperity contact, sealed fluid viscosity and the lubricant film thickness around the asperities respectively.
Substituting Eqs. (5) and (6) into Eq. (4) and rearranging the integral, the friction force acting on the free end of every single equivalent asperity is specified as follows:

$$F_{a-a} = f W \tag{7}$$

$$F_{f-a} = \mu \pi \frac{V}{h} r^2 \tag{8}$$

where W is normal contact load between a pair of asperities. Since higher asperity peaks subject to more bending stress caused by fluid flow, h in Eq. (8) is substituted with δ for the remainder of the paper. This implies that nonlinear interaction between the fluid flow and surface asperities is more significant for those asperities whose height is greater than d, as already discussed in Fig. 6.

3.2.2 Calculation of the strain energy released due to bending of a single asperity

Assuming asperities behave like an end-loaded cantilever beam, the elastic strain energy released during the dynamic bending of a single equivalent asperity is given by (adopted from the theory of mechanics of materials [44]) :

$$U_{iAE} = \int \frac{\sigma_b^{\,2}}{2E} dV_a \tag{9}$$

where E is equivalent elastic modulus given by Hertz theory, V_a is the volume of an equivalent asperity, and σ_b is the bending stress in deformation of an equivalent asperity that can be expressed as:

$$\sigma_b = \frac{M\,y}{I} \tag{10}$$

Where M is bending moment, y is distance from any point of the transverse section of bending to the neutral surface, and I is area moment of inertia. Setting:

$$dV_a = dA dx \tag{11}$$

Then the elastic strain energy released during the dynamic bending of any equivalent asperity with the height of x can be expressed as:

$$U_{iAE} = \frac{1}{2E} \iint (\frac{M\,y}{I})^2\, dA dx = \frac{1}{2EI} \int M^2\, dx \tag{12}$$

As it was assumed that elastic deformation (either due to direct contact or fluid flow) is more significant for those asperities whose heights is greater than d, therefore set $dx = d\delta$, the bending moment M can be evaluated by:

$$M = F\,\delta \tag{13}$$

If friction force remains constant (that means deformation radius is smaller than a critical value [43]) during elastic deformation of asperities, substituting Eq. (13) into Eq. (12) and rearranging the integral gives:

$$U_{iAE} = \frac{1}{2EI}\int (F\delta)^2 \, d\delta = \frac{F^2\delta^3}{6EI} \tag{14}$$

Substituting friction force, F, from Eqs. (7) and (8) into Eq. (14) results in elastic strain energy discharge for asperity-asperity (*a*-*a*) and fluid-asperity (*f*-*a*) interactions as following:

$$U_{iAE\,(a-a)} = \frac{f^2 W^2 \delta^3}{6EI} \tag{15}$$

$$U_{iAE\,(f-a)} = \frac{(\mu \pi V r^2)^2 \delta}{6EI} \tag{16}$$

3.2.3 Calculation of the mean strain energy released due to bending of a single asperity

Since $\delta = z - d$, thus the mean AE strain energy released in a single equivalent asperity deformation is given by:

$$\overline{U}_{iAE\,(a-a)} = \frac{f^2 W^2}{6EI} \frac{\int_d^\infty (z-d)^3 \, f(z)\, dz}{\int_d^\infty f(z)\, dz} \tag{17}$$

$$\overline{U}_{iAE\,(f-a)} = \frac{(\mu \pi V r^2)^2}{6EI} \frac{\int_d^\infty (z-d) \, f(z)\, dz}{\int_d^\infty f(z)\, dz} \tag{18}$$

3.2.4 Calculation of the total strain energy discharge

The total strain energy discharge in the elastic asperity deformations, U_{AE}, can be expressed as follows:

$$U_{AE} = A_a \, n \, \overline{U}_{iAE} \tag{19}$$

where A_a is the apparent deformation area and n is the number of deformations in unit area (given by Eq. (3)). Substituting Eqs. (17) and (18) into Eq. (19), the total strain energy discharge is given as following:

$$U_{AE(a-a)} = A_a D \frac{f^2 W^2}{6EI} \int_d^\infty (z-d)^3 f(z) dz \tag{20}$$

$$U_{AE(f-a)} = A_a D \frac{(\mu \pi V r^2)^2}{6EI} \int_d^\infty (z-d) f(z) dz \tag{21}$$

3.2.5 Calculation of the mean discharge time

The time needed for an equivalent asperity discharge can be calculated when deformation distance is divided by the sliding speed. Deformation distance, *L*, is estimated based on the equation available for displacement of free end (or maximum deflection) of the cantilever beams [44] by setting the length of beam as δ:

$$L = \frac{F\delta^3}{3EI} \tag{22}$$

Substituting Eqs. (7) and (8) into Eq. (22), the deformation distance is given by:

$$L_{a-a} = \frac{fW\delta^3}{3EI} = \frac{f\sqrt{r}\,\delta^{\frac{9}{2}}}{3I} \tag{23}$$

$$L_{f-a} = \frac{\mu \pi V r^2 \delta^2}{3EI} \tag{24}$$

It is noted that in Eq. (24), W was substituted with $\sqrt{r}\,E\,\delta^{\frac{3}{2}}$ from Hertz theory. The time needed for the discharge of an individual equivalent asperity deformation can be evaluated by the following expression:

$$t = \frac{2L}{V} \tag{25}$$

Hence, Substituting Eqs. (23) and (24) into Eq. (25) gives:

$$t_{a-a} = \frac{2f\sqrt{r}\,\delta^{\frac{9}{2}}}{3IV} \tag{26}$$

$$t_{f-a} = \frac{2\mu\pi r^2\delta^2}{3EI} \tag{27}$$

Substituting δ with $z-d$, the mean elastic discharge time is specified by:

$$\bar{t}_{a-a} = \frac{2f\sqrt{r}\int_d^\infty (z-d)^{\frac{9}{2}} f(z)\,dz}{3IV\int_d^\infty f(z)\,dz} \tag{28}$$

$$\bar{t}_{f-a} = \frac{2\mu\pi r^2\int_d^\infty (z-d)^2 f(z)\,dz}{3EI\int_d^\infty f(z)\,dz} \tag{29}$$

3.2.6 Calculation the rate of strain energy discharge

The total number of asperity deformations between two surfaces is expressed as follows:

$$N_{tot} = A_a D\int_d^\infty f(z)\,dz \tag{30}$$

In addition, an auxiliary function can be defined as [29,30,34]:

$$F_n(d^*) = \int_{d^*}^\infty (z^*-d^*)^n \phi(z^*)\,dz^* \tag{31}$$

where $z^* = \frac{z}{Rq}$ and $d^* = \frac{d}{Rq}$, and $\phi(z^*)$ is the standard height distribution of asperities. Eq. (31) indicates that $F_n(d^*)$ is influenced by the surface separation d and the characteristics of surface topography. Research has shown that the separation d is also determined by the surface topography and is independent of the load applied [40].

During sliding contact of mating faces, part of the kinetic energy is converted to the AE signals and the remainder of it is eventually dissipates to the surroundings in the form of thermal energy. Therefore, supposing that a portion K_e of the elastic strain energy is converted to AE pulses and the gain of the AE measurement system is K_g, dividing Eqs. (20) and (21) by Eqs. (28) and (29) respectively (and using Eqs. (30) - (31) to simplify the outcomes), the rate of strain energy release is given by:

$$\dot{U}_{AE(a-a)} = K_e K_g \frac{N_{tot} f W^2 V F_3(d^*)}{4E\sqrt{r}\, F_{\frac{9}{2}}(d^*)} \tag{32}$$

$$\dot{U}_{AE(f-a)} = K_e K_g \frac{\mu \pi r^2 N_{tot} V^2 F_1(d^*)}{4F_2(d^*)} \tag{33}$$

Eqs. (32) and (33) reveal that the release rate of elastic energy in dynamic bending of surface asperities is proportional to the number of asperity deformations, whether it is generated by direct asperity contact or by flow induced excitations. Moreover, the geometry of equivalent asperities, i.e. r, affcts the level of AE signals. Eq. (32) also confirms that the release rate of elastic energy in direct asperity contact is affected more by contact load rather than sliding speed. However, based on Eq. (33) sliding speed is more dominant in generating flow induced asperity excitations. In addition, as the term 'elastic' implies, the release rate of elastic energy in direct contact is affected by equivalent elastic modulus of mating asperities.

3.2.7 Calculation of the AE RMS

Substituting Eqs. (32) and (33) into Eq. (1) and considering the assumptions that have been made by F.Y.Edward et al.[30], the relationship between AE RMS value and the strain energy released can be expressed as following:

$$V_{rms(a-a)} = \frac{W}{2r^{\frac{1}{4}}} \sqrt{K_e K_g \frac{f N_{tot} V F_3(d^*)}{E F_{\frac{9}{2}}(d^*)}} \tag{34}$$

$$V_{rms(f-a)} = \frac{Vr}{2} \sqrt{K_e K_g \mu \pi N_{tot} \frac{F_1(d^*)}{F_2(d^*)}} \tag{35}$$

The direct asperity contact model presented in Eq. (34) matches well with the experimental work of F.Y.Edward et al. [30], where the attempt was made to prove the linear relationship between the contact load, W, and RMS value of AE signals in unlubricated conditions (boundary lubrication regime). Moreover, it contains elastic properties and frictional characteristics of sliding contact that has been addressed less frequently in previous works.

3.3 Viscous Friction Model

Lebeck [45] used a finite volume of fluid bounded within two arbitrary surfaces to characterise the general lubrication theory at the sealing interface. Using the equations developed by Lebeck in [45], Towsyfyan [20] showed that the component of shear stress acting in the sliding direction, τ_{zx} , is much greater than others. Therefore, the component of viscous friction force acting on any arbitrary differential element of fluid (Fig. 7) is given by:

$$dF = \tau_{zx}\, dA \tag{36}$$

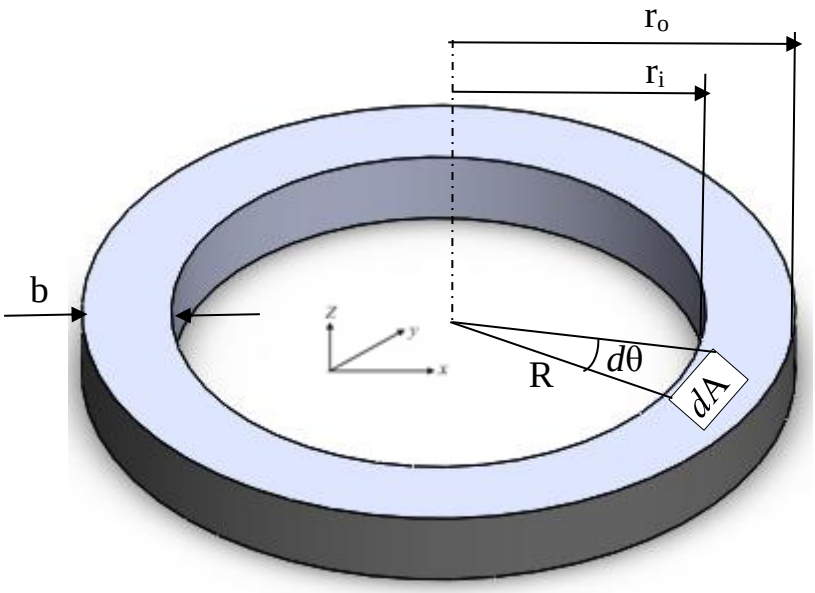

Fig. 7. Differential fluid element applied in viscous friction model

Where b is the seal width, r_i and r_o are the inside and the outside radius of the sealing interface respectively. R and θ represent the components of polar coordinate. AE is generated by shear of the differential elements of the fluid layers in the sealing gap, Fig.8.

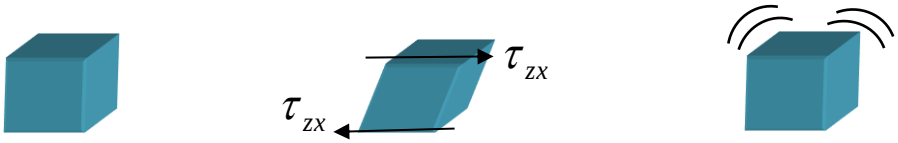

(a) Fluid element in rest (b) Sheared element (c) Energy released

Fig. 8. The concept of strain energy released due to viscous friction

Supposing that a portion K_e of the elastic strain energy is converted to AE pulses and the gain of the AE measurement system is K_g, the AE energy release rate at any arbitrary differential element of lubricant fluid can be evaluated by:

$$\dot{U}_{AE} = K_e K_g \iint V \, dF \tag{37}$$

Substituting dF from Eq. (36) into Eq. (37) and considering the maximum velocity component at sliding direction as V, rearranging double integral of Eq. (37) in polar coordinates will result in the rate of fluid born AEs in the sliding contact of mating surfaces:

$$\dot{U}_{AE} = K_e K_g \int_0^{2\pi} \int_{r_i}^{r_0} V \, \mu \frac{V}{h} \, R \, dR \, d\theta = 2\pi K_e K_g \, \mu \frac{V^2}{h} r_m \, b \tag{38}$$

where r_m is mean radius of sealing area. Substituting Eq. (38) into Eq. (1) and define constant parameters as $K = \sqrt{2\,\pi\, K_e\, K_g\, b\, r_m}$ reads:

$$V_{rms} = K \sqrt{\frac{\mu}{h}} V \tag{39}$$

Eq. (39) shows clearly that the viscous friction induced AE excitations are greater when rotational speed and lubricant viscosity are higher. However, this type of excitation has little connection with sealed pressure. It is immediately noted that the size of sealing gap, h, is a function of sliding speed itself, so that by increasing the sliding speed the size of sling gap is increased in the hydrodynamic lubrication regime. Therefore, flow induced asperity deformations remain the dominant AE source in the hydrodynamic lubrication regime. In the mixed lubrication regime, however, the size of sealing gap is kept in the range of average asperity heights and does not change significantly by the speed increase. Therefore it is logical to assume that by increasing the sliding speed in the mixed lubrication regime, the portion of viscous friction in an AE signal is increased.

4 Experimental Validation of the AE Model

Little information on condition monitoring of mechanical seals using industrial test rigs are available, e.g. see Ref [30]. In the literature most of the studies related to tribological AEs have been undertaken in the form of pin on disk or pin on cylinder in laboratories [46-48]. Fig. 9 shows the general view of the test rig designed and applied for condition monitoring of mechanical seals in this research. To ensure the test rig replicates the usual seal arrangement in practical applications such as pumps, real industrial mechanical seals rather than just pairs of face seal materials were employed.

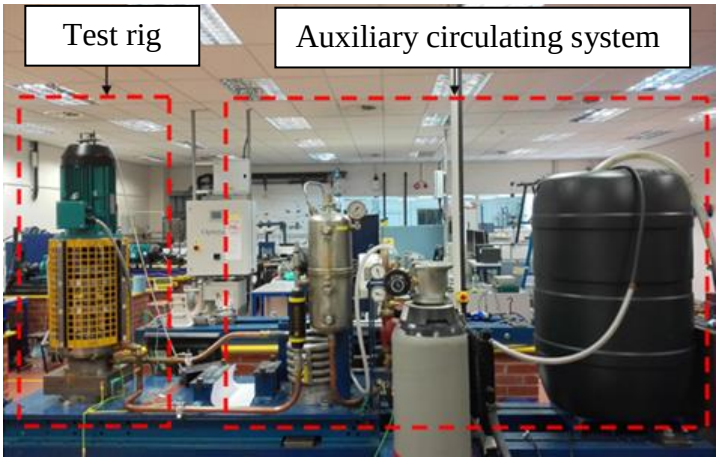

Fig. 9. General view of the mechanical seal test rig

An auxiliary circulating system was connected to the rig to pressurise the sealed fluid (water in this research) and take away the generated frictional heat as shown in Fig. 9. The auxiliary circulating system consists of several components such as (1) water container (2) circulating pumps, (3) radiator, (4) heat exchanger, (5) valves (6) cylinder of nitrogen gas to pressurise the water, (7) regulator on nitrogen cylinder (8) pressurised vessel, (9) pressure relief valve, (10) regulator and pressure sensor on the pressurised vessel and (11) flow meter, as arrowed in Fig. 10. Using this system, the tests were performed at a temperature around 26±2°C by circulating cooling water over the system.

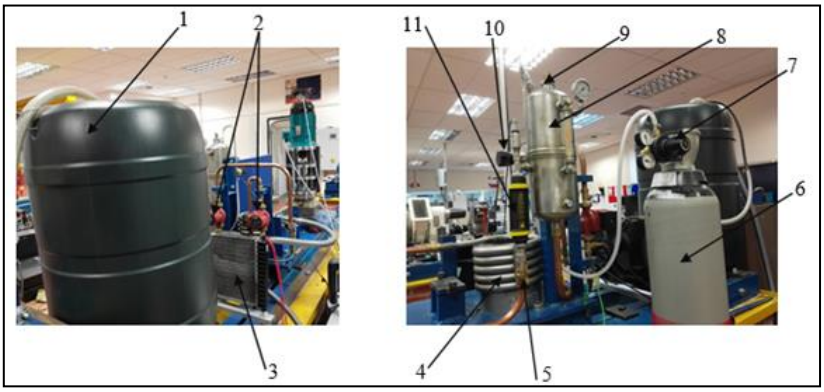

Fig. 10. Different components of the auxiliary circulating system

A John Crane Type 1648 MP pusher cartridge mechanical seal and a stainless-steel tube formed a pressurised chamber as shown schematically in Fig. 11 (a). A WD S/N FQ36 AE sensor with an operating frequency range from 100 kHz to 1MHz was employed to obtain the AE signals, allowing high frequency events due to frictional process to be monitored. The AE sensor has been located on the seal cartridge, close to the AE sources, to gain optimal results as shown schematically in Fig. 11 (b). Based on the primary understandings of this research, this position of AE sensor is less affected by transmission path and wave distortion which are a major problem in AE applications. The signal from an AE sensor is amplified and acquired by a 2 MHz high speed data acquisition system with 16-bit resolution. To record operational parameter's data such as rotational speed of shaft, temperature and sealed fluid pressure from related sensors, another 16-channel high speed data acquisition system at a sampling rate of 96 kHz has been used.

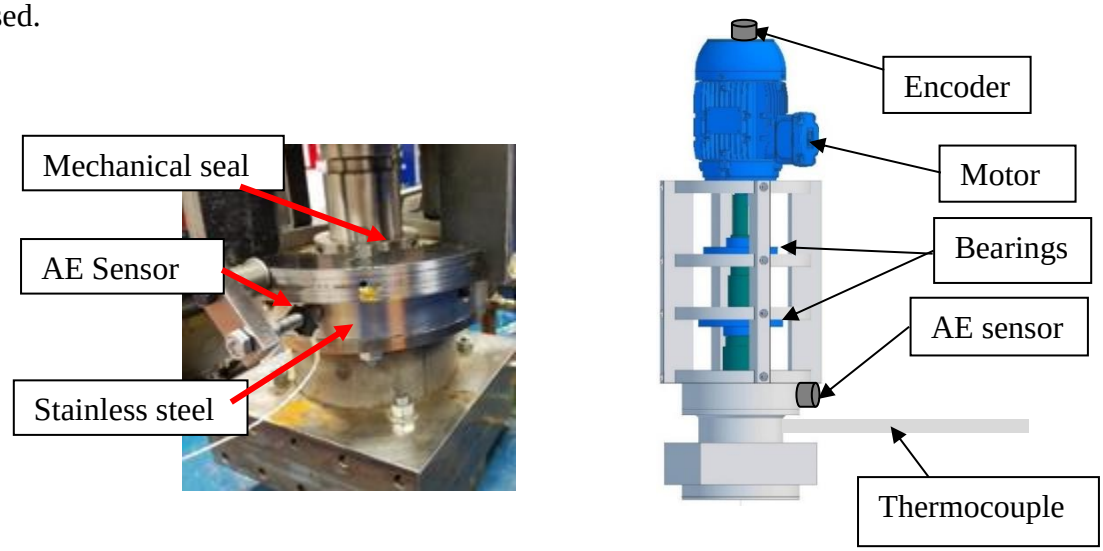

Fig.11. Configuration of the sensors on the rig, (a) AE sensor on pressurised chamber (b) Schematic illustration of the sensors on the rig

To identify the AE frequency range that can separate the tribological AEs from the background noises (e.g. motor vibration and element contact of bearings), a set of experiments has been carried out. For instance seal free test, which refers to idling of the rig when the seals were removed, was conducted to investigate the effect of background noises on the AE signatures. It was found that the tribological AEs are located in the range of 270±35 kHz. Thus, a band pass filter was designed using MATLAB codes and applied to AE data for remainder of the research. The details of such experiments are beyond the scope of present paper, interested readers are encouraged to see Ref [20] for more details.

Since mechanical seals are exposed to widely varying operating conditions during their service life, the experimental work in this research has been conducted at seven different sealed pressures from 2±0.05 bar to 8±0.05 bar with the step size of one bar, Fig. 12. For each load, the data has been recorded at ten different speeds of 120 rpm, 180 rpm, 240 rpm, 300 rpm, 360 rpm, 450 rpm, 600 rpm, 900 rpm, 1200 rpm and 1500 rpm to simulate different tribological regimes of mechanical seals. For each test AE raw signal was recorded continuously for 8 seconds.

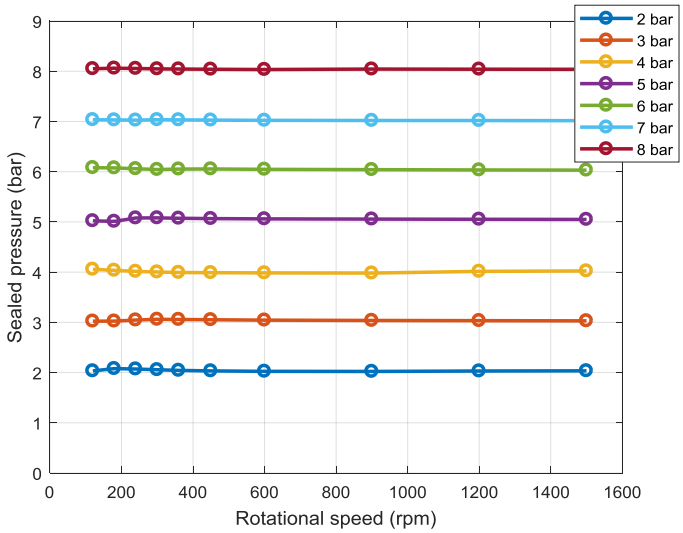

Fig.12. Sealed pressure during the tests, based on pressure sensor data

To ensure that the surface topography of seal faces meets the manufacturer's requirements, both rotating and stationary faces were examined before and after the tests, Fig. 13. It was proven that the seal faces were well polished and meet the requirements as prescribed in Appendix B. Also, no severe wear evidence was observed on completion of the tests.

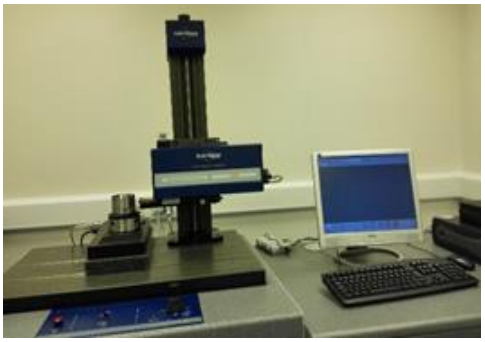

Fig. 13. Taylor Hobson Form Talysurf applied in this research

4.1 The Influence of Sliding Speed on AE RMS

AE source mechanisms interact with each other under different tribological regimes. Hence it is necessary to combine the developed equations and propose a comprehensive model that can explain the tribological behaviour of mechanical seals operating in different lubrication regimes.

(a) Modelling the mixed lubrication regime

Define all constant parameters of Eq. (34) as

$$K_1 = \frac{W}{2r^{\frac{1}{4}}} \sqrt{K_e K_g \frac{f F_3(d^*)}{E F_{\frac{9}{2}}(d^*)}} \tag{40}$$

The AE model presented in Eq. (34) can be simplified and expressed as:

$$V_{rms} = K_1 \sqrt{N_{tot} V} \tag{41}$$

In the mixed lubrication regime, direct asperity contact is confined by the shearing of lubricant between the mating asperities. Hence the theoretical model for the mixed lubrication regime is derived by considering the interaction of viscous friction and direct asperity collisions. Based on Eq. (38), the AE energy release rate generated by viscous friction increases with the sliding speed square. As it has been already discussed, see Section 3.3, other components of shear stress are negligible compared to the τ_{zx} that acts in the thickness direction of sealing gap. Therefore, it is logical to assume that the shearing rate of the lubricant film (confined between asperities in the ML region) is equal to the rate of asperity contact decrease. Consequently direct asperity collisions are limited with the same trend and hence the relationship between total number of contact asperities and sliding speed can be expressed as:

$$N_{tot} = \frac{K_2}{V^2} \tag{42}$$

Substituting Eq. (42) into Eq. (41) the relationship between AE RMS value and sliding speed in the mixed lubrication regime is prescribed by:

$$V_{rms} = \frac{K_3}{\sqrt{V}} = K_3 V^{-\frac{1}{2}} \tag{43}$$

Eq. (43) reveals that in the mixed lubrication regime (if other parameters are kept constant), the RMS value of AE signal is proportional to the reciprocal of square root of sliding speed (in other words, sliding speed power of -0.5).

(b) Modelling the hydrodynamic lubrication regime

Define all constant parameters of Eq. (35) as:

$$K_4 = \frac{r}{2} \sqrt{K_e K_g \mu \pi N_{tot} \frac{F_1(d^*)}{F_2(d^*)}} \tag{44}$$

The AE model presented for the hydrodynamic lubrication regime is simplified as follows:

$$V_{rms} = K_4 V \tag{45}$$

It is logical to assume that flow induced asperity deformation is dominant AE source mechanism, since the portion of viscous friction in an AE signal decreases when the size of sealing gap is increased in the hydrodynamic lubrication regime, as prescribed by Eq. (39).

Based on Eq. (45), a linear relationship exists between the sliding speed and the level of AE excitations in the hydrodynamic lubrication regime. It should be immediately noted that by increasing the sliding speed beyond a threshold, the sealing gap is increased more than the norm and therefore the stress field of fluid is not strong enough to generate elastic deformation in the surface asperities any more. In Fig. 14, a comparison of AE RMS values is made between the measured signal and predicted values when the rig operates under different sealed pressures.

The actual rotational speed of shaft was calculated based on the analysis of encoder data at the mean diameter of sealing interface. To achieve this, MATLAB codes have been developed to calculate the rotational speed of shaft and then convert it into the sliding speed based on the geometry of the sealing gap. The encoder has been synchronized with AE sensor to allow more accurate investigation on tribological behaviour of mechanical seals.

The constant parameters of K_3 and K_4 are adopted to the model (Eqs. (43) and (45) respectively) by statistical analysis carried out in MATLAB on the measured signals. To achieve this the best curves, in the form of power trend, have been fitted on the measured signals and the constant values were extracted directly from the software for each simulation. These values are then fed into developed models to simulate the predicted signals.

Fig. 14 is tribologically meaningful as it clearly agrees with the Stribeck curve. As it is observed, mixed and hydrodynamic lubrication regimes are identified using AE measurements. In addition, by increasing the sealed pressure, i.e. 8 bar, more direct asperity contact occurs and the boundary lubrication regime becomes dominant at lower speeds (i.e. speeds lower that 180 rpm).

Moreover, a good agreement is evident between the measured and predicted signals. It is clear that the developed models allow different tribological regimes to be indicated based on AE measurements that is critical in many engineering applications.

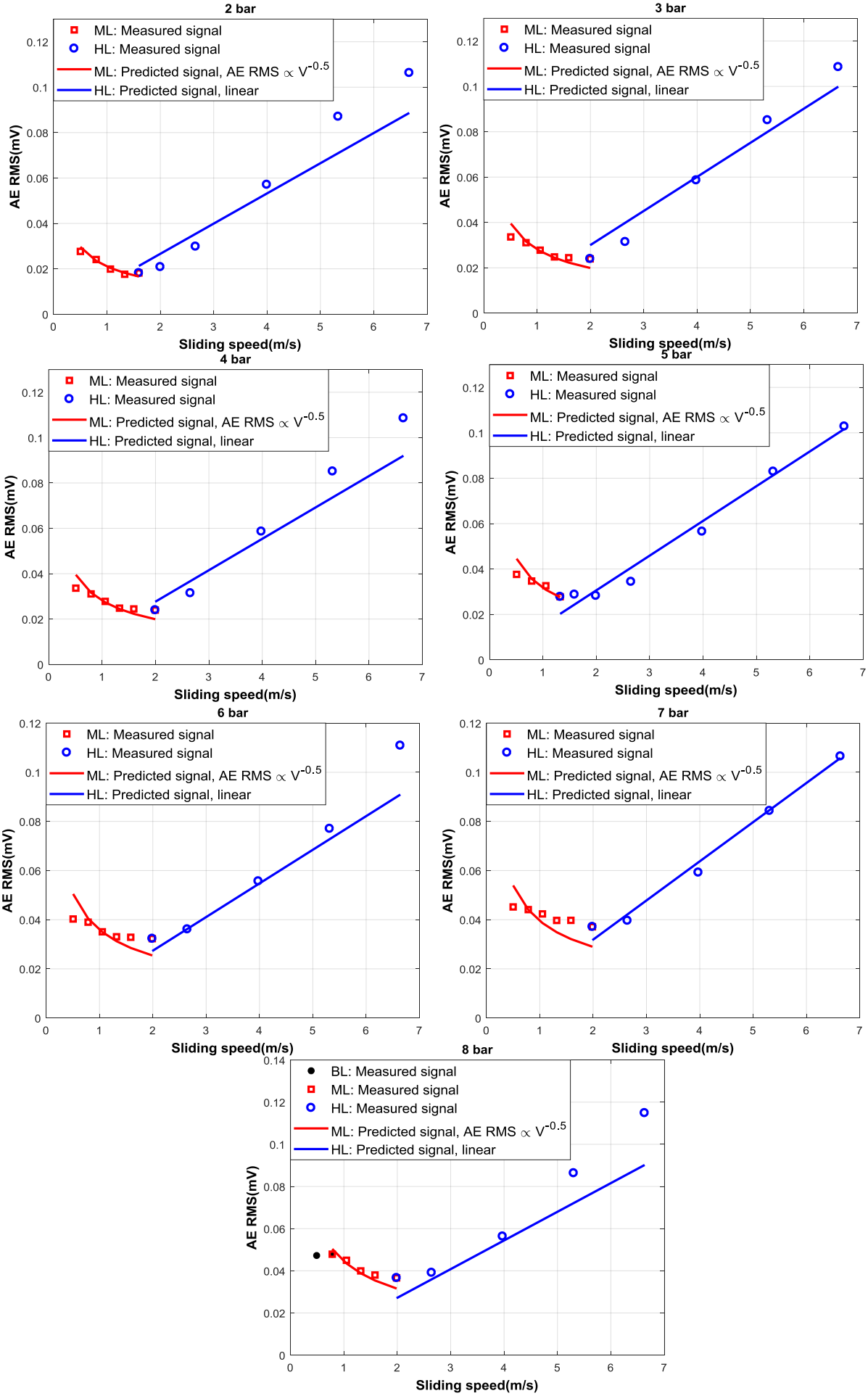

Fig.14. The relationship between AE RMS value and sliding speed

4.2 The Influence of Sealed Pressure on AE RMS

As prescribed by Eq. (34), AE RMS value is influenced by the contact load. However, this model cannot be applied to explain the recorded AE data since the load measured was the sealed fluid pressure rather than the load supported by asperity contacts. In general, it has been proven in the literature that the contact load is linearly proportional to the sealed pressure [20, 27]. This can be expressed mathematically as follows:

$$W = \alpha P + \beta \tag{46}$$

Where α and β are proportional constants. Substituting Eq. (46) for contact load into Eq. (34), and define all constant parameters as K_5, gives:

$$V_{rms} = K_5 P + B \tag{47}$$

Therefore, the AE RMS value varies linearly with the sealed pressure in mechanical seals. Fig. 15 presents the test results to validate the linear relationship between AE RMS value and sealed pressure when the seal operates at the constant speed of 120 rpm and under seven different loads, from 2 to 8 bar with the step size of 1 bar. It is logical to assume that running the rig at such a low rotational speed generates as many asperity collisions as possible.

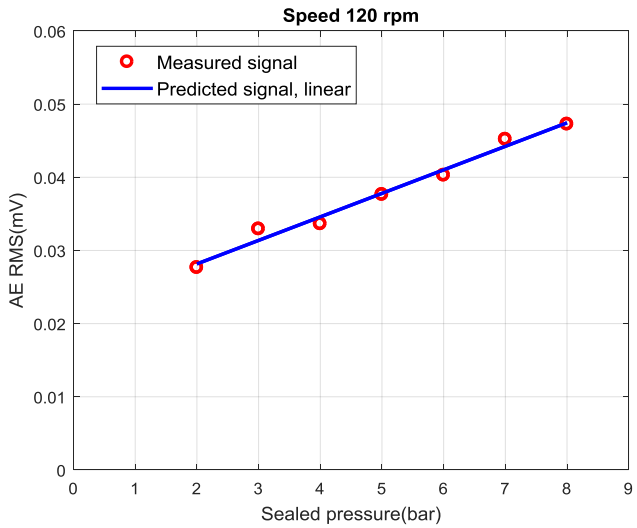

Fig.15. The relationship between AE RMS value and sealed pressure at speed of 120 rpm

4.3 Model Response to the Failure of Mechanical Seals

Different mechanisms such as dry running, erosion and corrosion may contribute to any damage to the mating faces and reduce the sealing performance of a mechanical seal. Consequently, higher values of leakage rate occur especially in transition point between mixed to hydrodynamic

lubrication regime where mechanical seals ideally operate. Under these conditions, if the sealed pressure drops to the minimum possible level and spring force is not powerful enough to compensate the opening forces, the opening forces overcome the closing forces and the mechanical seal fails. To demonstrate the efficiency of developed equations to diagnose such failure modes, some radial scratches were made on the mating ring as shown in Fig. 16. The smallest defect is only an artificially induced crack (approximately 6 *mm* length) and the biggest approximately 7×8 mm^2.

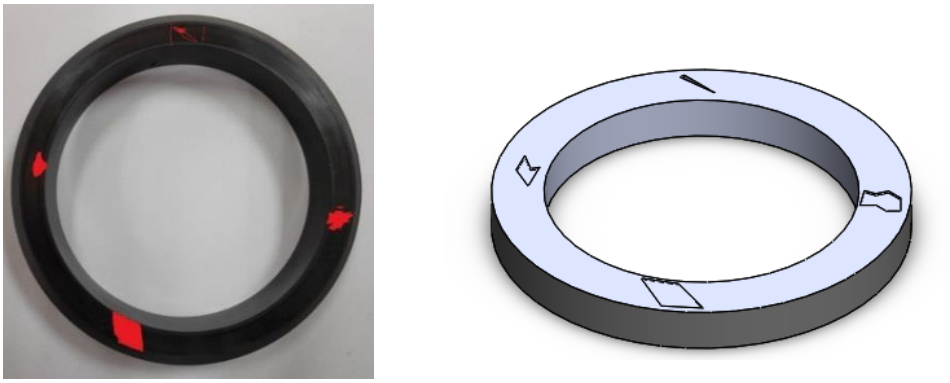

(a) (b)

Fig. 16. Defective seal (a) Scratches on stationary ring (b) Schematic illustration of artificially induced damages.

In Fig. 17, a comparison of AE RMS values is made between the measured signals (from the defective seal) and predicted values (for the healthy case) when the rig operates under different sealed pressures. The constant parameters of K_3 and K_4 are adopted to the model (Eqs. (43) and (45)) by statistical analysis carried out in MATLAB on the recorded signals from the defective seal test.

A significant difference is evident between the predicted signal and the values obtained in defective seal test for the hydrodynamic lubrication regime. Using Eq. (45), it was determined that a linear relationship exists between the sliding speed and RMS value of AE signals, this relationship has been validated in Section 4.1. However, that trend is not observed for the defective seal test. As illustrated in Fig.17, if the seal had not failed, then it would have generate AE levels as high as the predicted values for the hydrodynamic lubrication regime. This gives good evidence to detect the leakage which mainly refers to the failure of a mechanical seal.

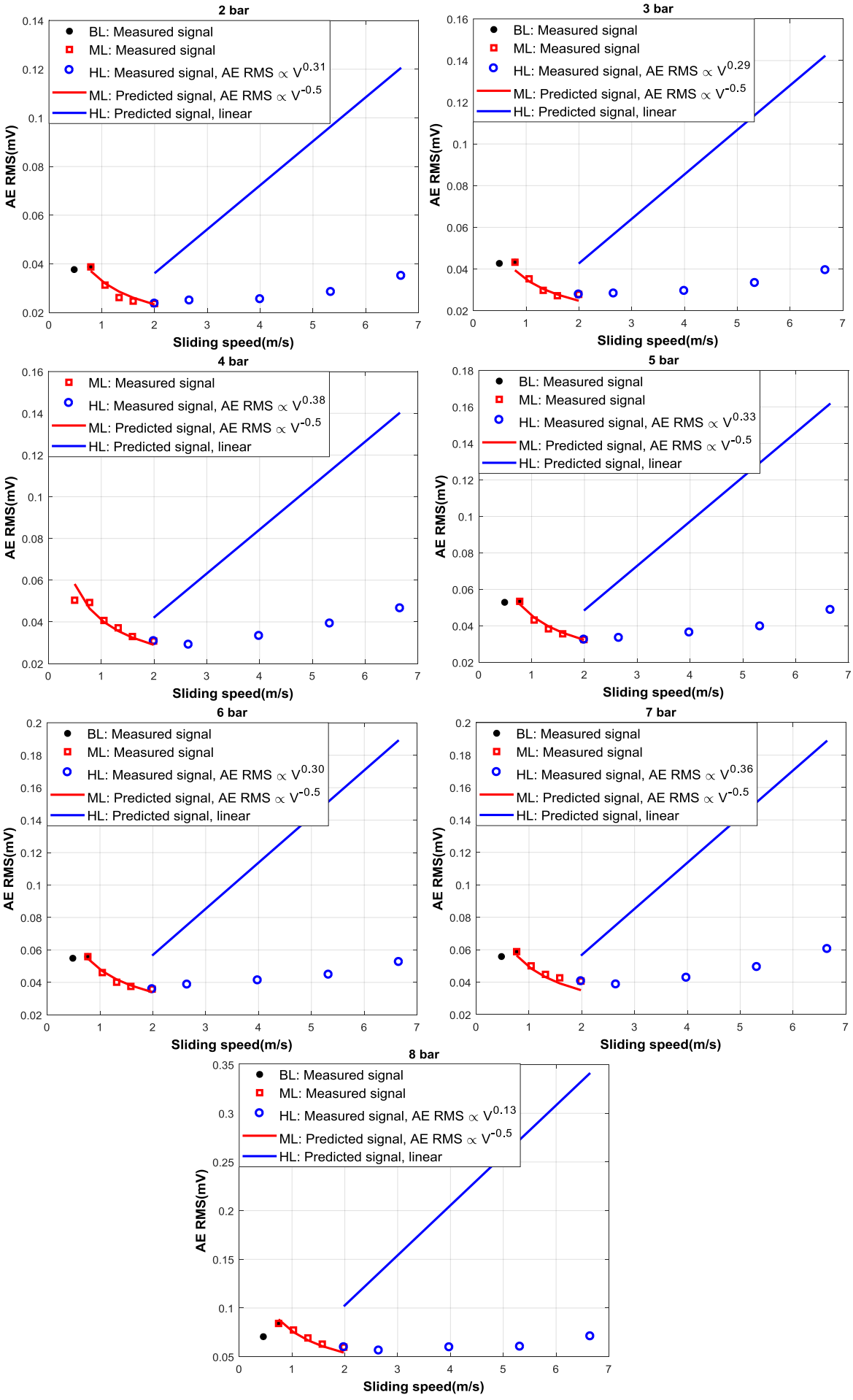

Fig.17. The relationship between AE RMS value and sliding speed in defective seal test

However, based on Fig. 17, the predicted signals achieved for sliding speed in the mixed lubrication regime is very close to the measured values. This shows that tribological behaviour of the scratched seal is similar to the healthy seal in the mixed lubrication regime and hence the same model response was generated. It is clear that in the most cases, an increase in the RMS value of AE signals is evident at the lowest speed. This indicates that boundary lubrication is dominant due to excessive wear in the scratched area when the rig operates at the speeds lower than 180 rpm. This trend that has not been observed in Fig. 14 (except for 8 bar sealed pressure) allows severe wear to be identified at lower speeds.

5 Conclusion

The paper developed a comprehensive model of the AE energy discharge under different tribological regimes of mechanical seals. To achieve this, different AE source mechanisms i.e. asperity collision, viscous friction and flow induced asperity deformation have been modelled based on seal operating parameters. From the developed models it was found that in direct asperity contact, the RMS value of AE signals is proportional to the coefficient of friction, sliding speed and contact load. In viscous friction and flow induced AE discharges, the effect of sliding speed is more dominant. In both cases the root mean square of AE signals increases linearly with sliding speed, also it is proportional with the square root of fluid viscosity. In all developed equations, topography of the mating surfaces, the size of sealing gap and asperity height distribution, play a key role.

To derive a comprehensive model that can explain the tribological behaviour of mechanical seals in the mixed and hydrodynamic lubrication regimes, the proposed equations for AE source mechanisms have been combined as the AE source mechanisms interact with each other under different tribological regimes. It has been proven that in the mixed lubrication regime the RMS value of AE signals is proportional to the sliding speed power of -0.5. In The hydrodynamic lubrication regime, however, a linear relationship was found between sliding speed and the AE RMS value if other parameters are constant. On this basis, any deviation from the predicted trends can be considered as a developing fault that may lead to failure of mechanical seals.

To demonstrate the efficiency of developed equations to diagnose failure of mechanical seals, some radial scratches were made on the mating ring to simulate leakage in the hydrodynamic lubrication regime. Based on the obtained results, a significant difference has seen observed between the measured and predicted signals in the hydrodynamic lubrication regime. This shows the strong potential of developed models to be used to obtain tribological behaviour of

mechanical seals and hence to develop reliable condition monitoring system under wide varying operating conditions.

References

1. Sadegh, H., A.N. Mehdi, and A. Mehdi, Classification of acoustic emission signals generated from journal bearing at different lubrication conditions based on wavelet analysis in combination with artificial neural network and genetic algorithm. Tribology International, 2016. 95: p. 426-434.
2. Towsyfyan, Hossein, Wei, Nasha, Gu, Fengshou and Ball, Andrew (2015), Identification of Lubrication Regimes in Mechanical Seals using Acoustic Emission for Condition Monitoring. The 54rd Annual Conference of the British Institute of Non-Destructive Testing BINDT 2015, 8th-10th September 2015, Telford, UK.
3. Miettinen, J. and V. Siekkinen, Acoustic emission in monitoring sliding contact behaviour. Wear, 1995. 181: p. 897-900.
4. Mba, D., et al., Application of acoustic emission technology for detecting the onset and duration of contact in liquid lubricated mechanical seals. Insight-Non-Destructive Testing and Condition Monitoring, 2006. 48(8): p. 486-487.
5. Raharjo, P., et al., An Investigation of Acoustic Emission Responses of a Self Aligning Spherical Journal Bearing. 2011.
6. Towsyfyan, H., et al., Characterization of Acoustic Emissions from Journal Bearings for Fault Detection. NDT 2013, 2013.
7. YOON, D.-J., et al., Early detection of damages in journal bearings by acoustic emission monitoring. Journal of acoustic emission, 1995. 13(1-2): p. 1-10.
8. Holenstein, A.P., Diagnosis of mechanical seals in large pumps. Sealing Technology, 1996. 1996(33): p. 9-12.
9. Márquez, F.P.G., et al., Condition monitoring of wind turbines: Techniques and methods. Renewable Energy, 2012. 46: p. 169-178.
10. Purarjomandlangrudi, A. and G. Nourbakhsh, Acoustic emission condition monitoring: an application for wind turbine fault detection. International Journal of Research in Engineering Technology, 2013. 2(5): p. 907-918.
11 Toutountzakis, T., C.K. Tan, and D. Mba, Application of acoustic emission to seeded gear fault detection. NDT & E International, 2005. 38(1): p. 27-36.

12. Loutas, T., et al., Condition monitoring of a single-stage gearbox with artificially induced gear cracks utilizing on-line vibration and acoustic emission measurements. Applied Acoustics, 2009. 70(9): p. 1148-1159.
13. Rogers, L., The application of vibration signature analysis and acoustic emission source location to on-line condition monitoring of anti-friction bearings. Tribology international, 1979. 12(2): p. 51-58.
14. Al-Ghamd, A.M. and D. Mba, A comparative experimental study on the use of acoustic emission and vibration analysis for bearing defect identification and estimation of defect size. Mechanical systems and signal processing, 2006. 20(7): p. 1537-1571.
15 Lubbinge, H., On the lubrication of mechanical face seals. 1999: Universiteit Twente.
16 Vezjak, A. and J. Vizintin, Experimental study on the relationship between lubrication regime and the performance of mechanical seals. Tribology & Lubrication Technology, 2001. 57(1): p. 17.
17 Tournerie, B. and J. Frene, Principal research areas on mechanical face-seals. Tribology international, 1984. 17(4): p. 179-184.
18 Lebeck, A., Mixed lubrication in mechanical face seals with plain faces. Proceedings of the Institution of Mechanical Engineers, Part J: Journal of Engineering Tribology, 1999. 213(3): p. 163-175.
19. Akay, A., Acoustics of friction. The Journal of the Acoustical Society of America, 2002. 111(4): p. 1525-1548.
20. H.Towsyfyan., Investigation of the nonlinear tribological behaviour of mechanical seals for online condition monitoring, PhD thesis, University of Huddersfield, 2017.
21. Assi, G.R., Mechanisms for flow-induced vibration of interfering bluff bodies. 2009, Imperial College London.
22. Bearman, P.W., Vortex shedding from oscillating bluff bodies. Annual review of fluid mechanics, 1984. 16(1): p. 195-222.
23. Alber, T., B. Gibbs, and H. Fischer, Characterisation of valves as sound sources: Fluid-borne sound. Applied Acoustics, 2011. 72(7): p. 428-436.
24. Drummond, C. and J. Israelachvili, Dynamic phase transitions in confined lubricant fluids under shear. Physical Review E, 2001. 63(4): p. 041506.
25. Mazuyer, D., et al., Friction dynamics of confined weakly adhering boundary layers. Langmuir, 2008. 24(8): p. 3857-3866.
26. Sinou, J.-J., J. Cayer-Barrioz, and H. Berro, Friction-induced vibration of a lubricated mechanical system. Tribology International, 2013. 61: p. 156-168.

27. Wangenheim, M. and M. Kröger, Avoidance of friction induced vibrations on seals. PAMM, 2008. 8(1): p. 10389-10390.
28 Fan, Y.E., Condition monitoring of mechanical seals using acoustic emissions. 2007, University of Manchester.
29 Sharma, R.B. and A. Parey, Modelling of acoustic emission generated in rolling element bearing. Applied Acoustics, 2017.
30 Fan, Y., F. Gu, and A. Ball, Modelling acoustic emissions generated by sliding friction. Wear, 2010. 268(5): p. 811-815.
31 Adams, G.G., S. Müftü, and N.M. Azhar. A Nano-Scale Multi-Asperity Contact and Friction Model. in ASME 2002 International Mechanical Engineering Congress and Exposition. 2002. American Society of Mechanical Engineers.
32 Benabdallah, H., Friction wear and acoustic emissions of some plastics sliding against Si 3 N 4. Wear, 2008. 264(1): p. 152-156.
33 Towsyfyan, H., et al., Characterization of Acoustic Emissions from Mechanical Seals for Fault Detection. 2014.
34 Archard, J., Contact and rubbing of flat surfaces. Journal of applied physics, 1953. 24(8): p. 981-988.
35 Boness, R. and S. McBride, Adhesive and abrasive wear studies using acoustic emission techniques. Wear, 1991. 149(1): p. 41-53.
36 Benabdallah, H. and D. Aguilar, Acoustic emission and its relationship with friction and wear for sliding contact. Tribology Transactions, 2008. 51(6): p. 738-747.
37 Boness, R., S. McBride, and M. Sobczyk, Wear studies using acoustic emission techniques. Tribology International, 1990. 23(5): p. 291-295.
38 Wang, L. and R. Wood, Acoustic emissions from lubricated hybrid contacts. Tribology International, 2009. 42(11): p. 1629-1637.
39 Huang, W., et al., An acoustic emission study on the starting and stopping processes of a dry gas seal for pumps. Tribology Letters, 2013. 49(2): p. 379-384.
40 Greenwood, J. and J. Williamson. Contact of nominally flat surfaces. in Proceedings of the Royal Society of London A: Mathematical, Physical and Engineering Sciences. 1966. The Royal Society.
41 Abdo, J. and K. Farhang, Elastic–plastic contact model for rough surfaces based on plastic asperity concept. International Journal of Non-Linear Mechanics, 2005. 40(4): p. 495-506.
42 Persson, B.N., Contact mechanics for randomly rough surfaces. Surface Science Reports, 2006. 61(4): p. 201-227.

43 Hurtado, J.A. and K.S. Kim. Scale effects in friction of single–asperity contacts. I. From concurrent slip to single–dislocation–assisted slip. in Proceedings of the Royal Society of London A: Mathematical, Physical and Engineering Sciences. 1999. The Royal Society.

44 Beer, F.P., et al., Mechanics of Materials, McGraw-Hill. 2006, Boston

45 Lebeck, A.O., Principles and design of mechanical face seals. 1991: John Wiley & Sons.

46 Hase, A., H. Mishina, and M. Wada, Correlation between features of acoustic emission signals and mechanical wear mechanisms. Wear, 2012. 292: p. 144-150.

47 Lingard, S., C. Yu, and C. Yau, Sliding wear studies using acoustic emission. Wear, 1993. 162: p. 597-604.

48 Hase, A., M. Wada, and H. Mishina, The relationship between acoustic emissions and wear particles for repeated dry rubbing. Wear, 2008. 265(5): p. 831-839.

Appendix A: Nomenclature

A	Area of a single equivalent asperity
A_a	Apparent deformation area
B	Proportional constants/Constant parameters
D	Number of asperity summits per unit area
E	Elastic modulus /Hertzian contact elastic modulus
F	Frictional force
$F_{(a-a)}$	Frictional force in asperity-asperity interactions
$F_{(f-a)}$	Frictional force in fluid-asperity interactions
$F_n(d^*)$	Auxiliary function
G	Duty parameter
I	Area moment of inertia
$K_{1,2,....}$	Proportional constants/Constant parameters
K_e	The portion of the elastic strain energy that is converted to AE
K_g	The gain of AE measurement system
L	Deformation distance
$L_{(a-a)}$	Deformation distance in asperity-asperity interactions
$L_{(f-a)}$	Deformation distance in fluid-asperity interactions
N_{tot}	Total number of asperity deformation
M	Dynamic bending moment
$p(z > d)$	The probability of asperity deformation
R	Radius of the curvature in the deformation area
Rq	Root mean square roughness
U_{AE}	AE energy released by acoustic emission sources
$\dot{U}_{AE}$	Rate of AE energy released
$\dot{U}_{AE(a-a)}$	Rate of AE energy released by asperity-asperity interactions

$\dot{U}_{AE(f-a)}$	Rate of AE energy released by fluid-asperity interactions
U_{iAE}	AE energy released by a single asperity
$U_{iAE(a-a)}$	AE energy released by asperity-asperity interactions
$U_{iAE(f-a)}$	AE energy released by fluid-asperity interactions
$\overline{U}_{iAE(a-a)}$	Mean AE strain energy released by asperity-asperity interactions
$\overline{U}_{iAE(f-a)}$	Mean AE strain energy released by fluid-asperity interactions
$\dot{U}_{AE(a-a)}$	Total strain energy discharge in asperity-asperity interactions
$\dot{U}_{AE(f-a)}$	Total strain energy discharge in fluid-asperity interactions
V	Sliding speed
V_a	Volume of an equivalent asperity
V_{rms}	RMS value of AE signal
$V_{rms(a-a)}$	RMS value of AE signal by asperity-asperity interactions
$V_{rms(a-a)}$	RMS value of AE signal by fluid-asperity interactions
W	Contact load in asperity collision
b	Seal width
d	Distance between the reference planes
f	Coefficient of friction
h	Lubricant film thickness
n	Number of asperity deformation in any unit area
r	Average radius of an equivalent asperity
r_i	Inside radius of sealing interface
r_o	Outside radius of sealing interface
r_m	Mean radius of sealing area
S	Sliding distance
t	Time needed for the discharge of asperity deformations
$t_{(a-a)}$	Time needed for the discharge of asperity-asperity interactions

$t_{(f-a)}$	Time needed for the discharge of fluid-asperity interactions
$\bar{t}$	Mean time needed for the discharge of asperity deformations
$\bar{t}_{(a-a)}$	Mean time for the discharge of asperity-asperity interactions
$\bar{t}_{(f-a)}$	Mean time for the discharge of fluid-asperity interactions
$z(x)$	Height of surface profile
α and β	Proportional constants
$\phi(z^*)$	Standard height distribution of asperities
δ	Elastic deflection of the asperities
μ	Viscosity
σ	Normal pressure in a single asperity contact
σ_b	Normal stress in bending of an equivalent asperity
τ	Shear stress
$\tau_{(a-a)}$	Shear stress in asperity-asperity interactions
$\tau_{(f-a)}$	Shear stress in fluid-asperity interactions
τ_{zx}	Component of shear stress acting in the sliding direction

APPENDIX B

Results of surface roughness measurements

Results of surface roughness measurements are presented in Tables B.1 and B.2.

Table B. 1 The results of roughness measurements

Sample number	Ra of stationary ring (µm)		Ra of rotating ring (µm)	
	Before tests	After Tests	Before tests	After Tests
1	0.0246	0.0104	0.0545	0.0309
2	0.0222	0.0082	0.0225	0.0193
3	0.0219	0.0107	0.0229	0.0346
4	0.0205	0.0104	0.0280	0.0308
5	0.0229	0.0095	0.0166	0.0342
6	0.0213	0.0096	0.0251	0.0474
7	0.0223	0.0097	0.0206	0.0518
8	0.0239	0.0104	0.0252	0.0104

Table B. 2 The results of waviness measurements

Sample number	W_t of stationary ring (µm)		W_t of rotating ring (µm)	
	Before tests	After Tests	Before tests	After Tests
1	0.1383	0.0677	0.2999	0.3227
2	0.1280	0.0660	0.8765	0.1227
3	0.1286	0.0724	0.2684	0.1793
4	0.1011	0.0732	0.3095	0.6303
5	0.1263	0.0749	0.1650	0.2706
6	0.1212	0.0828	0.2958	0.4211
7	0.1401	0.0726	0.2873	0.5113
8	0.1373	0.0646	0.6399	0.2504